Double-Diffusive Convection

Lecturer: Timour Radko
Notes written by: Christophe Gissinger & Toby Wood
Woods Hole Geophysical Fluid Dynamics Program 2008

27 June 2008

1 Introduction

Even in systems with a negative vertical density gradient, instability is possible if the density is controlled by two components (e.g. temperature T and salinity S) that diffuse at different rates [24]. In the oceans, temperature diffuses approximately 100 times faster than salt, and so many regions of the ocean are potential candidates for so-called "double-diffusive instability".

Doubly-diffusive effects were observed by several authors before Stern [24] explained the physical mechanism responsible. Jevons [4] and Ekman [1] had previously observed instability at the interface between temperature stratified water and an overlying layer of denser fluid, but neither recognised the significance of double-diffusion. Later, Stommel *et al.* [28] showed that a "perpetual salt fountain" can arise when a tube is inserted vertically through the interface between a layer of warm, salty water overlying cold, fresh water. The fountain persists until the system becomes well mixed. This experiment has recently been realised on an industrial scale [29].

There are two forms of double-diffusive instability, referred to as "salt fingers" and "diffusive convection".

1.1 Salt fingers

Suppose a fluid system contains positive vertical gradients of both temperature T and salinity S, such that the total density gradient is negative (i.e. stably stratified). We describe this configuration as "warm salty over cold fresh" (see Figure 1). In the absence of diffusive effects, a parcel of fluid displaced vertically downwards would find itself more buoyant than its surroundings, and therefore rise. However, if temperature diffusion is sufficiently strong, and salt diffusion sufficiently weak, then the parcel can come into thermal equilibrium with its surroundings before it rises, whilst still remaining salty. It therefore becomes less buoyant than its surroundings, and continues to fall under gravity. This process leads to "salt fingers" propagating down through the medium and, conversely, fresh fingers propagating upward (see Figure 2).

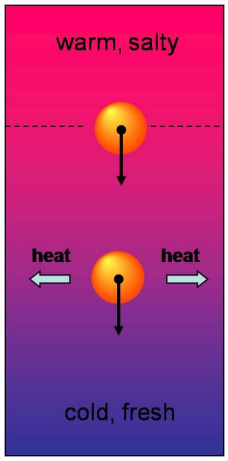

Figure 1: Schematic of the salt finger mechanism.

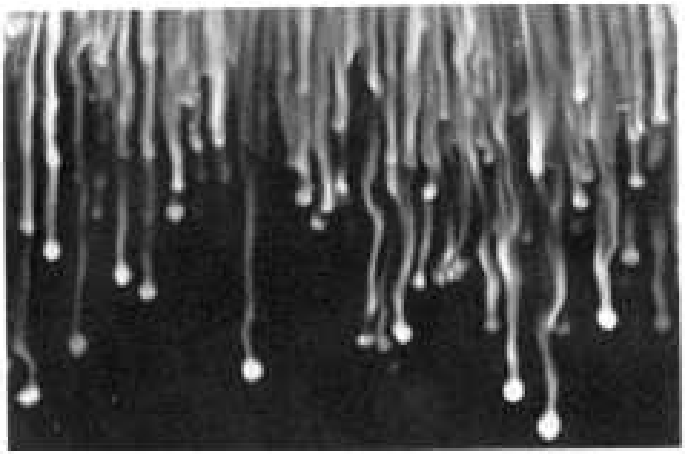

Figure 2: Salt fingers in a laboratory experiment [3].

1.2 Diffusive convection

Suppose we have negative vertical gradients of both T and S such that the total density gradient remains stably stratified, i.e. "cold fresh over warm salty"(see Figure 3). A parcel of fluid displaced vertically downwards now quickly absorbs heat by diffusion from its surroundings, and so "overshoots" when rising back through the medium. This leads to an oscillation of growing amplitude, i.e. an oscillatory instability.

Both kinds of double-diffusive instability are thought to play a role in small-scale mixing of the world's oceans. However, since the conditions necessary for salt fingers are more common, we focus here primarily on this instability.

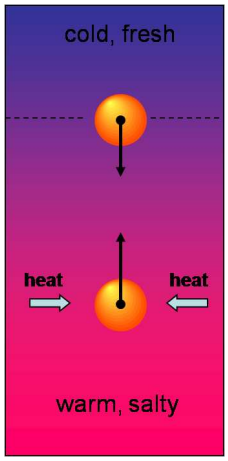

Figure 3: Schematic of the diffusive convection mechanism.

2 Mathematical formulation

2.1 The linear instability

We begin with the Boussinesq equations, which are valid over height scales less than the pressure and density scale heights, provided the flow speed remains much less than the sound speed.

$$0 = \nabla \cdot \mathbf{u}, \tag{1}$$

$$\frac{\partial \mathbf{u}}{\partial t} + \mathbf{u} \cdot \nabla \mathbf{u} = -\frac{1}{\rho_0}\nabla p - g\frac{\rho}{\rho_0}\hat{\mathbf{k}} + \nu \nabla^2 \mathbf{u}, \tag{2}$$

$$\frac{\partial T}{\partial t} + \mathbf{u} \cdot \nabla T = k_T \nabla^2 T, \tag{3}$$

$$\frac{\partial S}{\partial t} + \mathbf{u} \cdot \nabla S = k_S \nabla^2 S, \tag{4}$$

$$\frac{\rho - \rho_0}{\rho_0} = \beta(S - S_0) - \alpha(T - T_0). \tag{5}$$

Here, k_T and k_S represent diffusivity of heat and salt, ν is the kinematic viscosity and (ρ_0, p_0, T_0, S_0) denote the (constant) reference values of density, pressure, temperature and salinity.

We consider linear perturbations to a background state with $\overline{\mathbf{u}} = 0$, $\overline{T}_z \equiv \dfrac{d\overline{T}(z)}{dz} =$ const > 0, $\overline{S}_z \equiv \dfrac{d\overline{S}(z)}{dz} =$ const > 0 and $\dfrac{\partial \overline{p}}{\partial z} = -g\overline{\rho}$. (Overbars are used to denote unperturbed quantities, and primes will be used for their linear perturbations.) The background is stably stratified provided that density is decreasing with height, i.e.

$$\frac{1}{\rho_0}\overline{\rho}_z = \beta \overline{S}_z - \alpha \overline{T}_z < 0. \tag{6}$$

The perturbations then obey the equations

$$\begin{aligned} 0 &= \nabla \cdot \mathbf{u}', && (7)\\ \frac{\partial \mathbf{u}}{\partial t} &= -\frac{1}{\rho_0}\nabla p' - g\frac{\rho'}{\rho_0}\hat{\mathbf{k}} + \nu\nabla^2\mathbf{u}', && (8)\\ \frac{\partial T'}{\partial t} + w'\overline{T}_z &= k_T\nabla^2 T', && (9)\\ \frac{\partial S'}{\partial t} + w'\overline{S}_z &= k_S\nabla^2 S', && (10)\\ \frac{\rho'}{\rho_0} &= \beta S' - \alpha T'. && (11) \end{aligned}$$

Salt fingers typically exhibit much longer vertical scales than horizontal scales, so we seek solutions that are proportional to $\exp(\lambda t)\sin(k_1 x)\sin(k_2 y)$. We then obtain three algebraic equations relating λ to $\kappa^2 \equiv k_1^2 + k_2^2$:

$$\begin{aligned} \lambda w' &= -g(\beta S' - \alpha T') - \nu\kappa^2 w', && (12)\\ \lambda T' + w'\,\overline{T}_z &= -k_T\kappa^2 T', && (13)\\ \lambda S' + w'\,\overline{S}_z &= -k_S\kappa^2 S'. && (14)\\ & && (15) \end{aligned}$$

For given κ, there are three solutions for λ, one real and two complex conjugate. The complex solutions represent slowly decaying internal waves. The real solution represents double-diffusive instability if $\lambda > 0$. To determine the instability criterion, we analyse the marginal stability condition, $\lambda = 0$; we then find

$$g\left(\frac{\beta\overline{S}_z}{k_S} - \frac{\alpha\overline{T}_z}{k_T}\right) = \nu\kappa^4. \qquad (16)$$

This equation has solutions with $\kappa \in \mathbb{R}$ provided that the LHS is positive. The necessary condition for instability is therefore

$$R_\rho \equiv \frac{\alpha\overline{T}_z}{\beta\overline{S}_z} < \frac{k_T}{k_S}. \qquad (17)$$

The quantity R_ρ is called the *density ratio*. In the ocean, the diffusivities of temperature and salt are, respectively, $1.4 \times 10^{-7}\mathrm{m}^2\,\mathrm{s}^{-1}$ and $1.1 \times 10^{-9}\mathrm{m}^2\,\mathrm{s}^{-1}$, so instability requires $R_\rho \lesssim 100$. We also require $R_\rho > 1$ so that the background state is stably stratified (see equation (6)). The growth rate of the salt finger instability is greatest when $R_\rho \approx 1$.

2.2 Instability scales

We assume R_ρ is of order unity, in which case equation (16) implies

$$g\frac{\beta\overline{S}_z}{k_S} \sim g\frac{\alpha\overline{T}_z}{k_T} \sim \nu\kappa^4. \qquad (18)$$

The typical horizontal scale of the salt fingers is then d, where

$$d \sim \frac{2\pi}{\kappa} \sim 2\pi \left(\frac{k_T \nu}{g\alpha \overline{T}_z} \right)^{1/4} \tag{19}$$

For typical parameter values ($\alpha \sim 10^{-4}\mathrm{K}^{-1}$, $g \sim 10\mathrm{m\,s}^{-2}$, $\overline{T}_z \sim 0.01\mathrm{K\,m}^{-1}$, $\nu \sim 10^{-6}\mathrm{m}^2\,\mathrm{s}^{-1}$) we find $d \sim 0.06$m. The characteristic timescale and velocity for temperature diffusion are then $t \sim d^2/k_T \sim 10^4$s and $v \sim k_T/d \sim 10^{-5}\mathrm{m\,s}^{-1}$.

3 The role of salt fingers in the oceans

The necessary conditions for double-diffusive instability are common within the world's oceans (see Figure 4). In particular, 90% of the main Atlantic thermocline has density

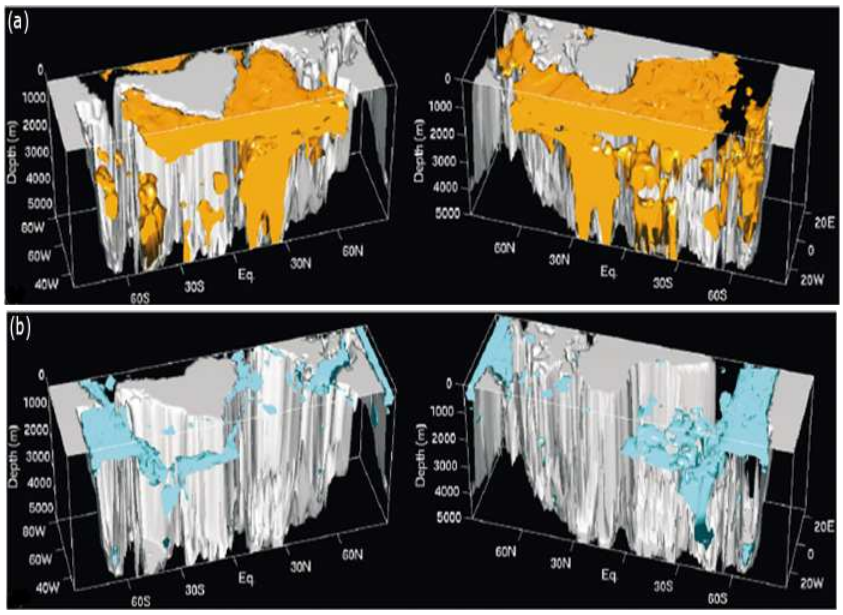

Figure 4: Regions of the ocean potentially susceptible to (a) salt fingers; (b) diffusive convection [35].

ratio $R_\rho < 2.3$, and is therefore strongly unstable to salt fingering. Shadowgraph imaging of the North Atlantic reveals finger-like structures with the centimetre horizontal scale characteristic of salt finger instability (see Figure 5).

Both salt fingers and diffusive convection are readily observed in laboratory experiments and numerical simulations. Importantly, salt fingers are found to be robust to interactions with internal gravity waves at Richardson numbers > 0.5. At smaller Richardson numbers, horizontal shear interrupts the vertical flux of heat and salt [27].

The main interest in salt fingers within the oceanographic community arises from their implications for vertical mixing [9, 22]. However, they may also explain the temperature–salinity patterns within the oceans (see Figure 6), and in particular the observed "thermohaline staircases" [26, 21]. Finally, salt fingers have been used to explain the lateral

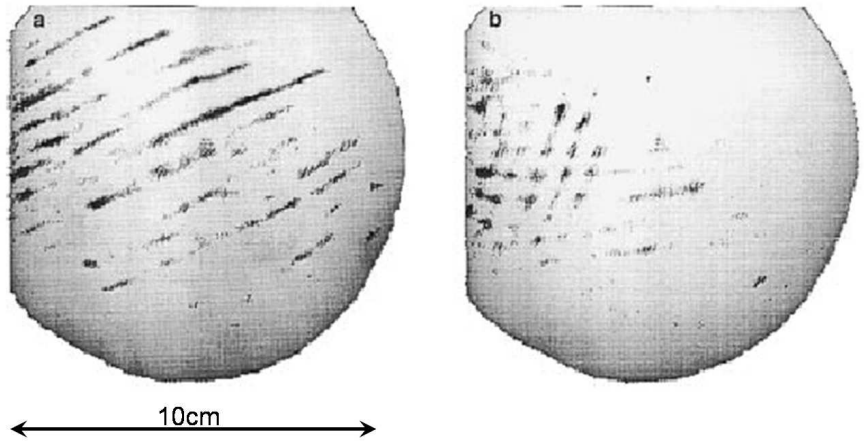

Figure 5: Shadowgraph images of the North Atlantic at 300m depth. The observed filaments are believed to be salt fingers, tilted by shear [9].

intrusions that are regularly observed in the ocean's temperature and salinity profiles [25].

4 The layered and smooth-gradient regimes of double-diffusive instability

Depending on the density ratio R_ρ, there are two different regimes of salt fingering. For larger values of R_ρ, both T and S have approximately linear vertical gradients, with small perturbations on the scale of the salt fingers. For smaller values of R_ρ, thermohaline staircases develop, with horizontal layers of approximately uniform temperature and salinity separated by thin interfaces (see Figure 7). The vertical scale of these layers is typically much larger than the scale of the fingers themselves, e.g. tens of metres in the ocean, and the transition between these two regimes occurs at around $R_\rho = 1.9$ [21].

Layers also form in numerical and laboratory experiments of oscillatory diffusive convection (see Figure 8). The layers merge until, perhaps, reaching a maximum size. Regarding the interfaces between layers as approximately laminar and steady, the (upward) fluxes of temperature and salt across an interface of thickness h are

$$F_T \sim k_T \frac{\Delta T}{h} \quad \text{and} \quad F_S \sim k_S \frac{\Delta S}{h}, \tag{20}$$

where ΔT and ΔS represent the total variations of temperature and salinity across the interface. The interface is stable provided that the total (upward) density flux, F_ρ, is negative, where $F_\rho = \rho_0(\beta F_S - \alpha F_T)$. We must therefore have

$$\frac{\beta \Delta S}{\alpha \Delta T} < \frac{k_T}{k_S}. \tag{21}$$

We would like to know what determines the vertical flux of T and S through the system and, in particular, how this depends on the density ratio R_ρ. We analyse the staircase and smooth-gradient regimes separately, seeking flux laws in either case.

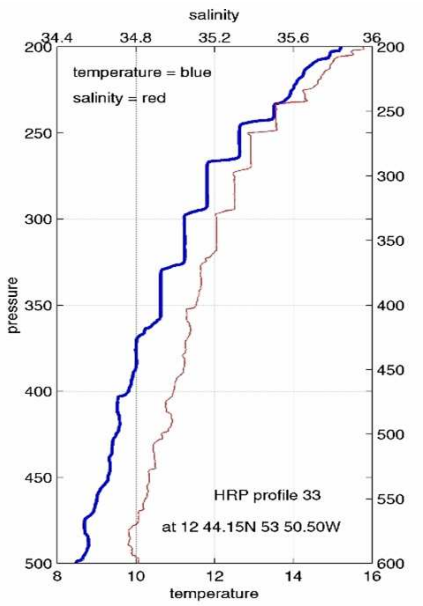

Figure 6: Temperature and salinity profiles in the West Atlantic near Venezuela.

4.1 The interfacial flux laws

We suppose that the fluxes of temperature and salt are determined by conditions within the interfaces, and independent of the height of the layers. By dimensional analysis, we conclude that the dimensionless temperature flux $\dfrac{F_T/(\Delta T)^{4/3}}{(g\alpha k_T)^{1/3}}$ can depend only on the dimensionless quantities $\dfrac{\alpha\Delta T}{\beta\Delta S}$, $\dfrac{\nu}{k_T}$ and $\dfrac{k_T}{k_S}$. This leads to Turner's 4/3 flux law [30]:

$$F_T, F_S \propto (\alpha\Delta T)^{4/3}. \tag{22}$$

Laboratory experiments typically exhibit an exponent slightly less than 4/3, though it is unclear to what extent these experiments can be extrapolated to describe the ocean [20, 10, 6, 7]. The hypothesis that temperature and salinity fluxes in the ocean are independent of layer thickness has been tested by Wilson [34]; if the ocean's thermohaline staircases are in a steady state, then the fluxes, and hence the temperature variations, should be the same across each interface. Figure 9 shows the variation of $\alpha\Delta T$ and $\beta\Delta S$ with layer thickness for a typical Ice-Tethered Profiler (ITP) observation in the Arctic. The observation supports Turner's key assumption that temperature and salt fluxes are not correlated with the thickness of the layers.

4.2 The gradient flux laws

In the smooth-gradient regime, we are concerned with perturbations to a background state that has linear profiles of T and S. After non-dimensionalising with respect to the scales

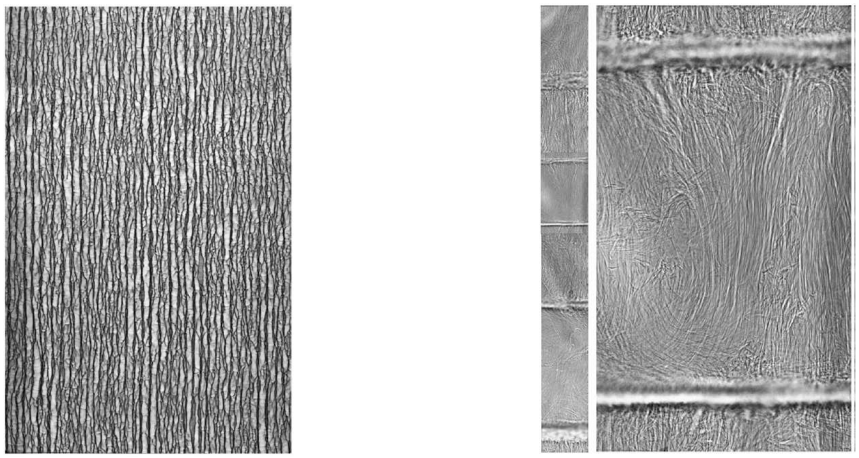

Figure 7: The gradient and staircase regimes of salt fingers [7].

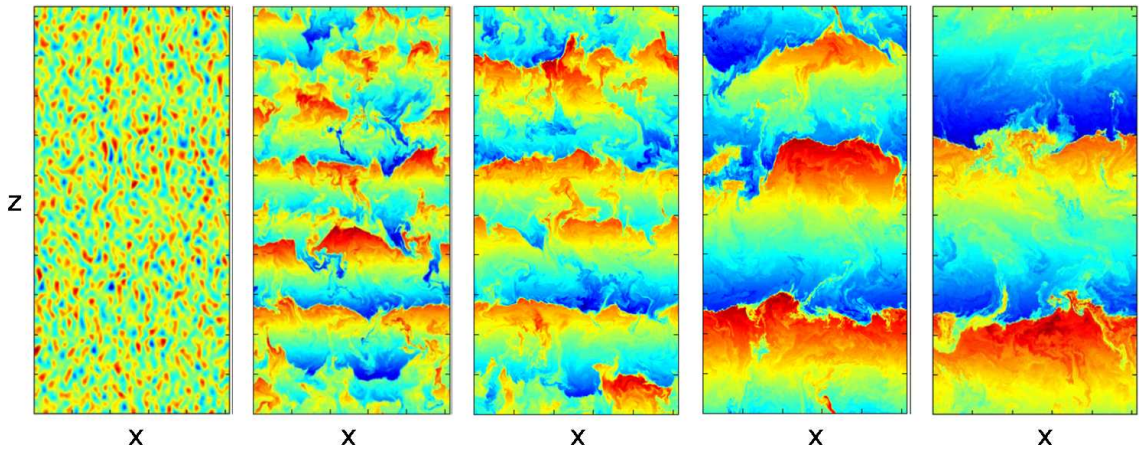

Figure 8: The formation of layers in diffusive convection [12]. The colour shows the departure of temperature from a uniform gradient.

obtained for the linear perturbations, we are left with the equations

$$0 = \nabla \cdot \mathbf{u}, \tag{23}$$

$$\frac{1}{\mathrm{Pr}}\left[\frac{\partial \mathbf{u}}{\partial t} + \mathbf{u}\cdot\nabla\mathbf{u}\right] = -\nabla p + (T-S)\hat{\mathbf{k}} + \nabla^2\mathbf{u}, \tag{24}$$

$$\frac{\partial T}{\partial t} + \mathbf{u}\cdot\nabla T + w = \nabla^2 T, \tag{25}$$

$$\frac{\partial S}{\partial t} + \mathbf{u}\cdot\nabla S + \frac{w}{R_\rho} = \tau\nabla^2 S, \tag{26}$$

where $\tau = k_S/k_T$ is the Lewis number and $\mathrm{Pr} = \nu/k_T$ is the Prandtl number. From these equations, we conclude that the dimensionless temperature and salt fluxes can depend only

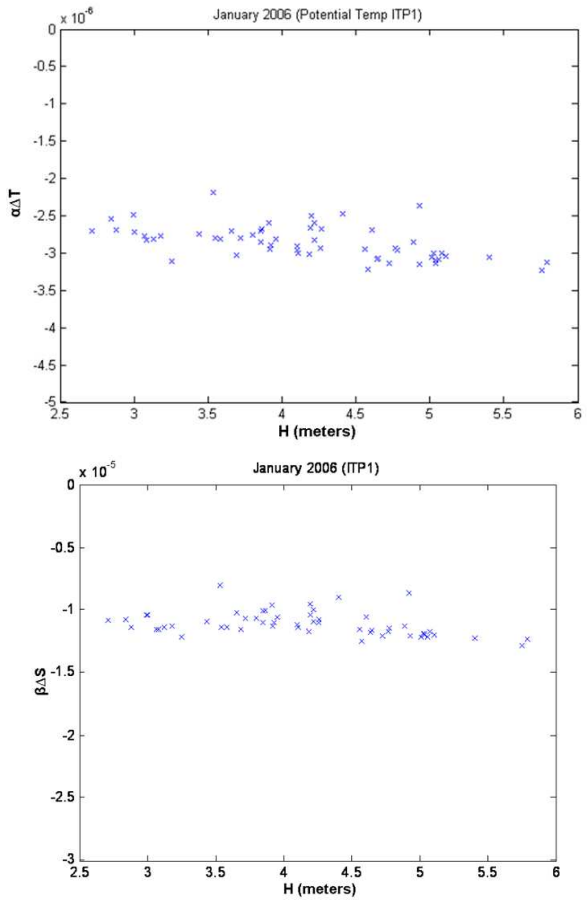

Figure 9: Temperature and salinity changes across interfaces between layers of thickness H.

on the dimensionless numbers R_ρ, τ and Pr. In particular, we can write

$$\frac{-F_T}{k_T \overline{T}_z} = \mathrm{Nu}(R_\rho, \tau, \mathrm{Pr}), \tag{27}$$

where Nu is the Nusselt number. Regarding the diffusivities as fixed, we would like to determine the variation of the Nusselt number with the density ratio R_ρ. Stern [26] noted that salt fingers can excite gravity waves and conjectured that this would lead to a collective instability of the salt finger regime when the Stern number $A = \dfrac{\beta F_S - \alpha F_T}{\nu(\alpha \overline{T}_z - \beta \overline{S}_z)}$ becomes order unity, in which case the nonlinear regime would be characterised by $A \approx 1$. However, the results of laboratory experiments suggest that the Stern number varies with Prandtl number. Observations of heat–salt fingers typically yield $A = O(1)$, $\mathrm{Pr} \approx 7$ and $\tau \approx 0.01$, whereas sugar–salt fingers have $A \sim 0.001 - 0.1$, $\mathrm{Pr} \approx 1000$ and $\tau \approx 1/3$ [23, 8, 2, 7].

5 Asymptotic analysis of the fingering regime

5.1 Sugar–Salt fingers

Within the high-Prandtl number regime relevant to sugar–salt fingers we can justify neglecting the inertial terms in equation (24). The problem is also simplified by the narrow range of unstable density ratios ($1 < R_\rho < \tau^{-1} \approx 3$). Several authors [31, 32, 13, 5, 14, 18] have undertaken a weakly nonlinear analysis of the marginally unstable modes. The following model is based on an expansion in which $\epsilon = \left(\frac{1}{\tau R_\rho} - 1\right)$ is small [19]. The space and time scales arise from the linear theory, and so we define $\mathbf{x} = \epsilon^{-1/4}\mathbf{x}_0$ and $t = \epsilon^{-3/2}t_0$. The remaining quantities scale as

$$\begin{aligned} \mathbf{u} \sim \mathbf{x}/t \sim \epsilon^{5/4} \\ \nabla^2 T \sim \nabla^2 S \sim w \sim \epsilon^{5/4} \\ \Rightarrow (T, S) \sim \epsilon^{3/4} \\ \nabla p \sim \nabla^2 \mathbf{u} \\ \Rightarrow p \sim \epsilon^{3/2} \end{aligned}$$

After expanding the equations in powers of ϵ, the leading order balances are

$$T_0 = S_0 \tag{28}$$

$$w_0 = \nabla_0^2 T_0 = \nabla_0^2 S_0 \tag{29}$$

and the second order balances are

$$\nabla_0 p_0 = (T_1 - S_1)\hat{\mathbf{k}} + \nabla_0^2 \mathbf{u}_0 \tag{30}$$

$$\frac{\partial T_0}{\partial t_0} + \nabla_0 \cdot (\mathbf{u}_0 T_0) + w_1 = \cancel{2\nabla_0 \cdot \nabla_1 T_0} + \nabla_0^2 T_1 \tag{31}$$

$$\frac{1}{\tau}\left[\frac{\partial S_0}{\partial t_0} + \nabla_0 \cdot (\mathbf{u}_0 S_0)\right] + w_0 + w_1 = \cancel{2\nabla_0 \cdot \nabla_1 S_0} + \nabla_0^2 S_1 \tag{32}$$

$$\tag{33}$$

After eliminating all second order terms, we are left with a closed system of asymptotic equations:

$$(\frac{1}{\tau} - 1)\left[\frac{\partial T_0}{\partial t_0} + \nabla_0 \cdot (\mathbf{u}_0 T_0)\right] = (\nabla_0^4 - 1)\nabla_0^2 T_0 - \frac{\partial}{\partial z_0}\nabla_0^2 p_0 \tag{34}$$

$$\left(\frac{\partial^2}{\partial x_0^2} + \frac{\partial^2}{\partial y_0^2}\right) p_0 = -\frac{\partial}{\partial z_0}\nabla_0^4 T_0 \tag{35}$$

$$\nabla_0^2 u_0 = \frac{\partial p_0}{\partial x_0} \tag{36}$$

$$\nabla_0^2 v_0 = \frac{\partial p_0}{\partial y_0} \tag{37}$$

The power law scaling for the heat flux is therefore $\langle wT \rangle \sim w_0 T_0 \sim \epsilon^2$. Similarly, the thermal variance and density flux are found to scale as $\langle T^2 \rangle \sim \epsilon^{3/2}$ and $\langle w\rho \rangle \sim \epsilon^{5/2}$ respectively.

In this weakly nonlinear framework, the saturation of the double-diffusive instability can be explained in terms of triad interactions between the various normal modes. Numerical simulations of the 2D equations roughly reproduce the asymptotic prediction; the scaling laws within the numerical results are estimated to be

$$\langle wT \rangle \sim \epsilon^{1.73} \quad \left\langle T^2 \right\rangle \sim \epsilon^{1.43} \quad \langle w\rho \rangle \sim \epsilon^{2.71}. \tag{38}$$

5.2 Heat–Salt fingers

For Heat–salt fingers, the Prandtl number is ≈ 7, so we cannot neglect inertial effects. Also, the density ratio in the oceans is typically close to unity, so weakly nonlinear models are unlikely to be of much relevance. Instead, Radko [17] examined the strongly nonlinear regime, with $\delta = \sqrt{1 - R_\rho^{-1}} \ll 1$. Two dimensional numerical simulations of this regime show "modons", small coherent vortex pairs that seem to be largely responsible for the transport of heat and salt (see Figure 10). In the limit $\delta \to 0$, an explicit solution for a

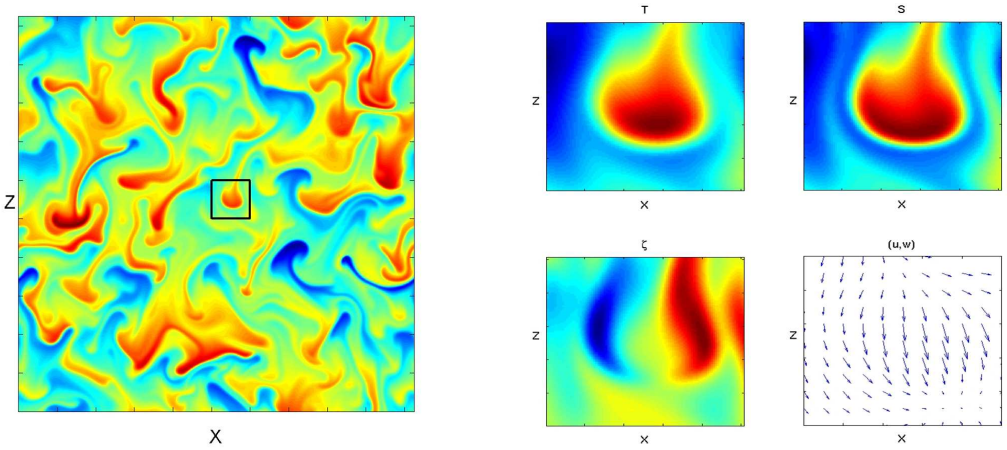

Figure 10: Stongly nonlinear heat–salt fingers in 2D, and properties of a single "modon".

circular, rectilinearly propagating modon can be found, in polar coordinates, by expanding in powers of δ. The solutions have $w \sim \delta^{-3/4}$ and $T, S \sim \delta^{-1/4}$, so that $F_T, F_S \sim 1/\delta$, assuming that the modons dominate transport. Again, 2D numerical simulations are roughly in agreement with the asymptotic theory.

6 Thermohaline Staircases

One of the most intriguing aspects of double diffusive convection is its ability to transform smooth vertical gradients into a stepped structure consisting of mixed layers separated by thin stratified interfaces. These layers have great significance for small-scale mixing in the oceans; tracer release experiments in the North Atlantic central thermocline suggest that the presence of layers increases the effective diffusivity by salt fingers from $0.1\text{cm}^2\,\text{s}^{-1}$ to $1\text{cm}^2\,\text{s}^{-1}$ [22, 33, 27, 9]. Staircases are routinely observed in regions where the density ratio is $R_\rho < 1.9$ [21], but their origin is still poorly understood. Several questions can be raised:

- What is the origin of thermohaline staircases?
- What are the conditions for staircase formation?
- What sets the vertical scale of the layers?

6.1 Explanation of layer formation

Several hypotheses have been put forward to explain the origin of thermohaline staircases, e.g. [26, 11]. Here, we look at the suggestion by Radko [15] that layers formation arises from an instability of the flux gradient laws. A secondary instability then allows layers to merge, until the staircase achieves a stable vertical scale. This mechanism can be tested against numerical simulations of staircase formation (see Figures 11 and 12).

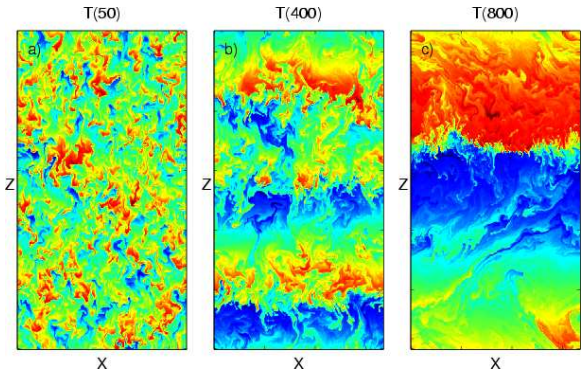

Figure 11: Formation and evolution of layers in a numerical experiment. The temperature field is shown at $t = 50$, $t = 400$ and $t = 800$.

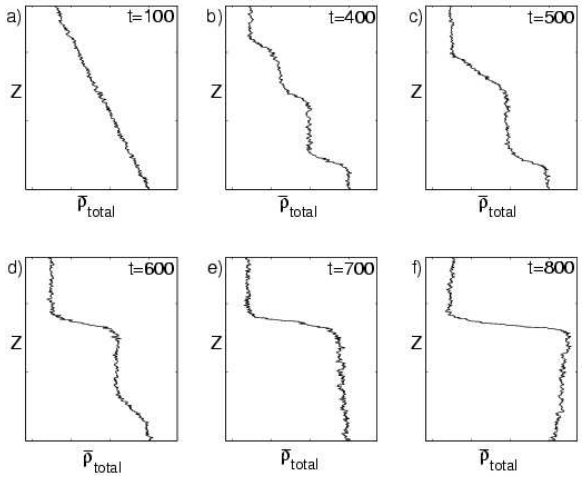

Figure 12: Total x-averaged density for the same simulation as in Figure 11 at $t = 100$, 400, 500, 600, 700, 800.

6.2 Instability of a uniform gradient

After averaging over small-scale variations of T and S, we have (1D) conservsation equations

$$\frac{\partial T}{\partial t} = -\frac{\partial}{\partial z} F_T \tag{39}$$

$$\frac{\partial S}{\partial t} = -\frac{\partial}{\partial z} F_S \tag{40}$$

We suppose that the Nusselt number Nu and flux ratio γ depend only on the local density ratio R_ρ:

$$\frac{F_T}{-k_T T_z} = \mathrm{Nu}(R_\rho) \tag{41}$$

$$\frac{\alpha F_T}{\beta F_S} = \gamma(R_\rho) \tag{42}$$

We now consider small (linear) perturbations (T_1, S_1, R_1) to a background state (T_0, S_0, R_0) with uniform gradient in T and S. The qualitative form of $\gamma(R_\rho)$ is indicated schematically in Figure 13. In the weakly unstable regime as $R_\rho \to 1/\tau$, the flux ratio must become

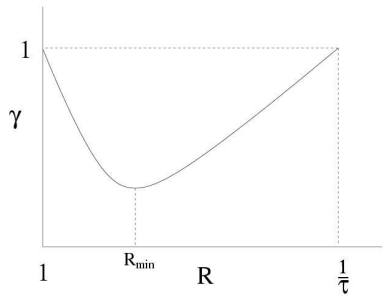

Figure 13: Dependence of the flux ratio γ on the density ratio R

unity. In the strongly unstable regime as $R_\rho \to 1$ we expect "eddy mixing" to render both temperature and salt fluxes equal. Experiments at intermediate values of R_ρ suggest that γ may obtain a minimum < 1 for some $R_\rho = R_{\min}$ [20].

A normal mode analysis for perturbations of the form $(T_1, S_1) \propto \sin(kz)\exp(\lambda t)$ yields an eigenvalue equation for the growth rate λ:

$$\lambda^2 + \lambda\left(D_2 + \mathrm{Nu}(R_0) - D_1 \mathrm{Nu}(R_0) R_0 - \frac{R_0 D_2}{\gamma(R_0)}\right) k^2 - D_1 \mathrm{Nu}^2(R_0) k^4 / R_0 = 0 \tag{43}$$

where

$$D_1 = \left.\frac{\partial(1/\gamma)}{\partial R}\right|_{R_\rho = R_0} R_0 \tag{44}$$

and

$$D_2 = \left.\frac{\partial(\mathrm{Nu})}{\partial R}\right|_{R_\rho = R_0} R_0. \tag{45}$$

So the basic uniform gradient is linearly unstable if $D_1 > 0$, i.e. if γ *decreases* with increasing R_ρ. If the dependence of γ on R_ρ is of the form shown in Figure 13 then instability is present for any $R_\rho < R_{\min}$. The physical mechanism responsible for this instability is sketched in Figure 14. With R_ρ and γ as shown, there is a convergence of heat flux in the lower domain, amplifying the perturbation to the background linear temperature gradient. In the nonlinear regime, this instability produces well-defined layers and interfaces.

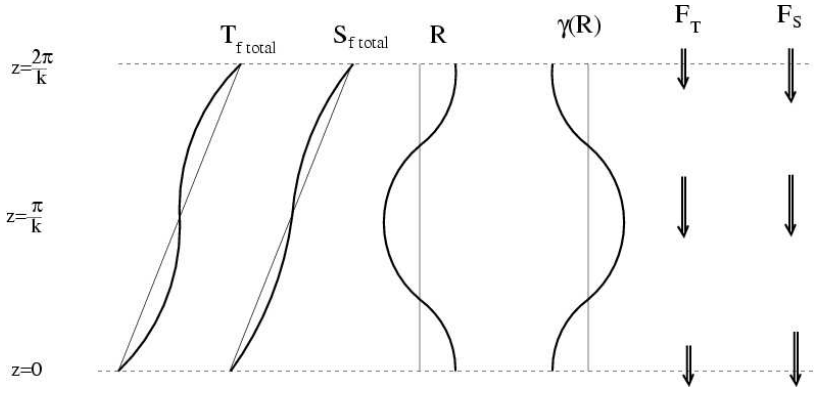

Figure 14: The physical mechanism behind the γ-instability. A decrease in γ with R results in the growth of the perturbation to a uniform T–S gradient.

To test whether variations of γ are essential for the formation of layers, we turn to the results of numerical simulations. If we define ρ_f as the horizontal average of the full (nonlinear) perturbation of density to the uniform background gradient, then we can write

$$\int \rho_f \frac{\partial \rho_f}{\partial t}\, dz = \int \rho_f \frac{\partial}{\partial z}(F_T - F_S)\, dz \tag{46}$$

$$\Rightarrow \frac{d}{dt}\int \frac{\rho_f^2}{2}\, dz = \int \rho_f (1 - \frac{F_S}{F_T})\frac{\partial}{\partial z} F_T\, dz + \int \rho_f F_T \frac{\partial}{\partial z}(-\frac{F_S}{F_T})\, dz \tag{47}$$

$$\equiv I_{\mathrm{Nu}} + I_\gamma \tag{48}$$

where the integrals I_{Nu} and I_γ respectively quantify the effects of variation in heat flux and flux ratio. The values of I_{Nu} and I_γ were continuously recorded in the course of a numerical simulation and the results are shown in Figure 15. We see that I_{Nu} typically makes a negative contribution to the density variance, so a positive contribution from I_γ is essential for the formation of layers.

6.3 Merger of thin layers

Numerical simulations suggest that the layers formed by the γ-instability are not steady. The second process in the creation of staircases is the merger of thin layers, increasing the T and S variations across each interface. To explain the observed layer interaction, we

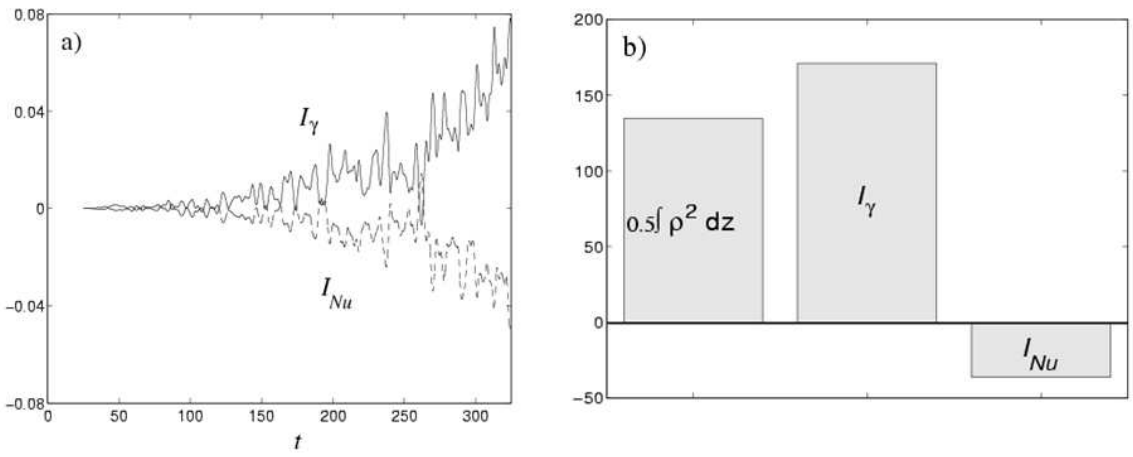

Figure 15: Balance of terms in the density variance equation (48). (a) The time evolution of I_γ and $I_{\rm Nu}$, indicated by solid and dashed lines. (b) Time integrals of I_γ and $I_{\rm Nu}$ over the period of layer formation.

now consider the stability of a series of salt finger interfaces. As illustrated by Figure 16, we perturb the temperature profile, making alternate interfaces weaker and stronger. The

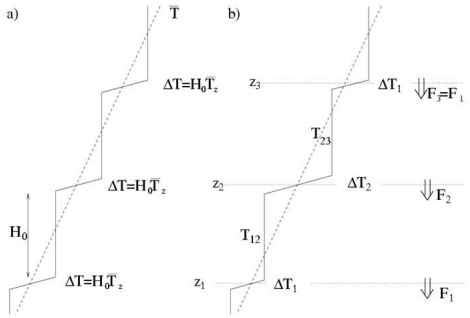

Figure 16: Temperature profiles of an infinite series of interfaces, taken from [16]. (a) Unperturbed state with equal steps (b) Perturbed state in which the T–S jumps at the even interfaces are decreased, and the jumps at odd interfaces are increased.

temperatures of the layers then evolve according to

$$H\frac{\partial}{\partial t}T_{12} = F_{T2} - F_{T1} \tag{49}$$

$$H\frac{\partial}{\partial t}T_{23} = F_{T3} - F_{T2} \tag{50}$$

We calculate the temperature fluxes across each interface using Turner's 3/4 flux law: $F_T = C(R_\rho)(\Delta T)^{4/3}$ (see §4.1). Assuming that $(\Delta T_1 - \Delta T_2) \ll \Delta T$ and $(\Delta S_1 - \Delta S_2) \ll \Delta S$

we perform a normal mode analysis, which results in an eigenvalue problem for the growth rate λ:

$$\lambda^2 + \lambda(...) - \left.\frac{\partial(\gamma^{-1})}{\partial R_\rho}\right|_{R_\rho=R_0} \frac{64T_{0z}^{2/3}}{3H^{4/3}} C^2(R_0)k^4 = 0 \tag{51}$$

As before, there exists a positive root of this equation if $\dfrac{d(1/\gamma)}{dR_\rho} > 0$, so the equally stepped state is unstable if γ is a decreasing function of R_ρ.

6.4 Equilibration of thermohaline staircases

We have yet to explain the mechanism that halts the merging of the layers, and thus sets the scale of the observed steady staircases. To do this, we augment the analysis of §6.3 with convective dynamics, parameterised by the convective flux law $\mathrm{Nu}_L = C_L \mathrm{Ra}_\rho^{0.2}$ [7]. This situation is illustrated by Figure 17. We now find that layers become stable above a certain

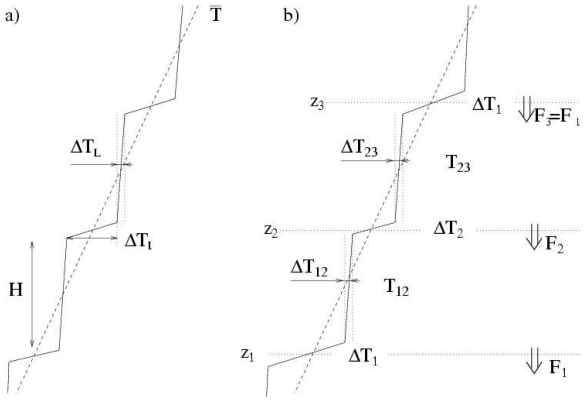

Figure 17: Temperature profiles of an infinite series of interfaces [16], including convective fluxes across each layer (c.f. Figure 16).

critical height, H_{cr}, given by

$$H_{\mathrm{cr}} = \left(\frac{C_L}{C}\right)^{15/8} \frac{\left(\frac{R_{\min}}{R_0}-1\right)^{9/4}\left(\frac{R_{\min}}{\gamma_{\min}}-1\right)^{1/4}}{\left(\frac{R_{\min}}{\gamma_{\min}}-\frac{R_{\min}}{R_0}\right)^{5/2}} \left(\frac{1}{\gamma_{\min}}-1\right)^{3/8} \left(\frac{k_T \mathrm{Nu}}{g\alpha T_{0z}}\right)^{1/4}. \tag{52}$$

Numerical simulations of the parameterised (1D) equations [16] demonstrate both the initial instability of the uniform gradient and the secondary merging instability (see Figure 18). The merging events halt when the layers become larger than the predicted critical height H_{cr}.

7 Future challenges

Although progress has been made in quantifying the effect of double diffusion on temperature flux, we are still lacking a unified theory for the whole parameter space. Little is known

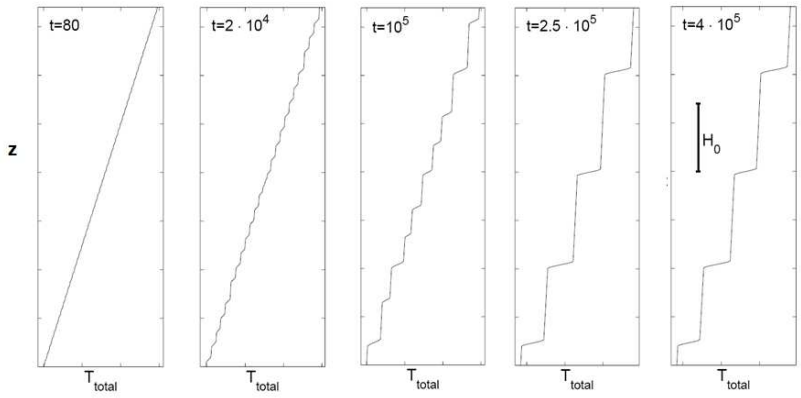

Figure 18: Results of a 1D simulation including parameterisations for both salt fingers and convection (taken from [16]).

regarding the dependence of the Nusselt number on the Lewis number or Prandtl number. The large-scale consequences of double diffusion have also not been fully studied, such as its role in controlling the T–S relation, diapycnal velocity and lateral mixing. Further analysis is required to predict and explain the magnitude and dynamics of thermohaline intrusions. Finally, there are unanswered questions regarding the modification of double-diffusive instability in the presence of shear, waves and turbulence, and the nature of the salt finger anisotropy.

References

[1] V. W. Ekman, *On dead water*, Scientific Results of the Norwegian North Polar Expedition, 1893-1896, 5 (1906), pp. 1–152.

[2] R. W. Griffiths and B. Ruddick, *Accurate fluxes across a salt-sugar finger interface deduced from direct density measurements*, J. Fluid Mech., 99 (1980), pp. 85–95.

[3] H. E. Huppert and J. S. Turner, *Double-diffusive convection*, J. Fluid Mech., 106 (1981), p. 299.

[4] W. S. Jevons, *On clouds; their various forms, and protruding causes*, Sydney Magazine of Science and Art, 1 (1858), pp. 163–176.

[5] T. M. Joyce, *Marginally unstable salt fingers: limits to growth*, Journal of Marine Research, 40 (Suppl.) (1982), pp. 291–306.

[6] D. E. Kelley, *Fluxes through diffusive staircases: A new formulation*, Journal of Geophysical Research, 95 (1990), pp. 3365–3371.

[7] R. Krishnamurti, *Double diffusive transports in laboratory thermohaline staircases*, J. Fluid Mech., 483 (2003), pp. 287–314.

[8] R. B. Lambert and J. Demenkow, *On the vertical transport due to fingers in double diffusive convection*, J. Fluid Mech., 54 (1972), pp. 627–640.

[9] L. S. Laurent and R. W. Schmitt, *The contribution of salt fingers to vertical mixing in the north atlantic tracer release experiment*, Journal of Physical Oceanography, 29 (1999), pp. 1404–1424.

[10] T. J. McDougall and J. R. Taylor, *Flux measurements across a finger interface at low values of the stability ratio*, Journal of Marine Research, 42 (1984), pp. 1–14.

[11] W. J. Merryfield, *Origin of thermohaline staircases*, J. Phys. Oceanogr., 30 (2000), pp. 1046–1068.

[12] I. Prikasky, *Direct numerical simulations of the diffusive convection and assessment of its impact on artic climate change*, Thesis, (2007).

[13] M. R. E. Proctor, *Steady subcritical thermohaline convection*, J. Fluid Mech., 105 (1981), pp. 507–521.

[14] M. R. E. Proctor and J. Y. Holyer, *Planform selection in salt fingers*, J. Fluid Mech., 168 (1986), pp. 241–253.

[15] T. Radko, *A mechanism for layer formation in a double diffusive fluid*, J. Fluid Mech., 497 (2003), pp. 365–380.

[16] T. Radko, *What determined the thickness of layers in a thermohaline staircase?*, J. Fluid Mech., 523 (2005), pp. 79–98.

[17] ——, *The double-diffusive modon*, J. Fluid Mech., 609 (2008), pp. 59–85.

[18] T. Radko and M. Stern, *Finite-amplitude salt fingers in a vertically bounded layer*, J. Fluid Mech., 425 (2000), pp. 133–165.

[19] T. Radko and M. E. Stern, *Salt fingers in three dimensions*, J. Mar. Res., 57 (1999), pp. 471–502.

[20] R. W. Schmitt, *Flux measurements on salt fingers at an interface*, Journal of Marine Research, 37 (1979), pp. 419–436.

[21] ——, *Form of the temperature salinity relationship in the central water: evidence for double-diffusive mixing*, Journal of Physical Oceanography, 11 (1981), pp. 1015–1026.

[22] R. W. Schmitt, J. R. Ledwell, E. T. Montgomery, K. L. Polzin, and J. M. Toole, *Enhanced diapycnal mixing by salt fingers in the thermocline of the tropical atlantic*, Science, 308 (5722) (2005), pp. 685–688.

[23] C. Y. Shen, *Heatsalt finger fluxes across a density interface*, Physics of Fluids A, 5 (1993), pp. 2633–2643.

[24] M. E. Stern, *The "salt-fountain" and thermohaline convection*, Tellus, 12 (1960), pp. 172–175.

[25] ——, *Lateral mixing of water masses*, Deep-Sea Research, 14 (1967), pp. 747–753.

[26] ——, *Collective instability of salt fingers*, J. Fluid Mech., 35 (1969), pp. 209–218.

[27] M. E. Stern, T. Radko, and J. Simeonov, *3-d salt fingers in an unbounded thermocline with application to the central ocean*, Journal of Marine Research, 59 (2001), pp. 355–390.

[28] H. Stommel, A. B. Aarons, and D. Blanchard, *An oceanographic curiosity: the perpetual salt fountain*, Deep-Sea Res., 3 (1956), pp. 152–153.

[29] K. Tsubaki, S. Maruyama, A. Komiya, and H. Mitsugashira, *Continuous measurement of an artificial upwelling of deep seawater induced by the perpetual salt fountain*, Deep-Sea Res., Part I, 54 (2007), pp. 75–84.

[30] J. S. Turner, *Salt fingers across a density interface*, Deep-Sea Res., 14 (1967), pp. 499–611.

[31] G. Veronis, *On finite amplitude instability in thermohaline convection*, Journal of Marine Research, 23 (1965), pp. 1–17.

[32] ——, *Effect of a stabilizing gradient of solute on thermal convection*, J. Fluid Mech., 34 (1968), pp. 315–336.

[33] ——, *Updated estimate of double diffusive fluxes in the c-salt region*, Deep Sea Research Part I: Oceanographic Research Papers, 54 (2007), pp. 831–833.

[34] A. Wilson, *Structure and dynamics of the thermohaline staircases in the beaufort gyre*, Naval Postgraduate School Thesis, (2007).

[35] Y. You, *A global ocean climatological atlas of the turner angle: Implications for double-diffusion and water-mass structure*, Deep-Sea Res., 49 (2002), pp. 2075–2093.